Journal of Electroceramics, 7, 113–120, 2001

The Electrical and Defect Properties of $Bi_3Zn_2Sb_3O_{14}$ Pyrochlore: A Grain-Boundary Phase in ZnO-Based Varistors

JANE CLAYTON,[1,*] HITOSHI TAKAMURA,[1,†] RENAUD METZ,[2] HARRY L. TULLER[1] & BERNHARDT J. WUENSCH[1]

[1]*Crystal Physics and Electroceramics Laboratory, Department of Materials Science and Engineering, Massachusetts Institute of Technology, Cambridge, MA 02139, USA*

[2]*Laboratoire Hydrazines et Procédés, UCBL-CNRS-SNPE, Bâtiment 731 – Berthelot, 43 Boulevard du 11 Novembre, 69 622 Villeurbanne, France*

Submitted April 18, 2001; Revised September 4, 2001; Accepted September 4, 2001

Abstract. The electrical conductivity of $Bi_3Zn_2Sb_3O_{14}$ pyrochlore was studied as a function of temperature and partial pressure of oxygen. Conductivity measurements by ac complex impedance analysis and ionic transference number measurements show this pyrochlore to be a mixed ionic-electronic conductor with an energy band gap of 3.15 ± 0.9 eV. A defect model in which Frenkel defects on the oxygen lattice are dominant is confirmed. Enthalpies of reduction, oxidation and the sum of oxygen vacancy formation and migration were found to be 4.82 ± 0.8 eV, 1.48 ± 1.0 eV and 1.67 ± 1.0 eV respectively.

Keywords: electrical conductivity, ionic transference number, mixed conductor, varistor, grain boundary barriers

Introduction

The nonlinear current-voltage relationship exhibited by ZnO that contains Bi_2O_3, CoO, Sb_2O_3 and other additives forms the basis for its use as a varistor in surge protectors. This nonohmic behavior results from the segregation of second phases at grain boundaries [1]. These additives interact in complex ways to serve various functions: Bi_2O_3 melts during processing, thus allowing liquid-phase sintering [2, 3]; Co leads to development of interface states [3] that insure the development of sufficiently high space-charge barriers at the grain boundaries. The presence of Sb derived from the addition of Sb_2O_3 controls microstructure through formation of a secondary spinel phase, $Zn_7Sb_2O_{12}$, that impedes grain growth [2–4]. However, these oxide additions also result in the formation of another secondary phase at grain boundaries: a pyrochlore shown to have composition $Bi_3Zn_2Sb_3O_{14}$. The phase was first identified by Wong [4] who employed dilute $HClO_4$ to selectively dissolve the ZnO matrix [5] of specimens that had compositions related to commercial varistor materials. The residual grain-boundary phases consisted of well-formed octahedra and a skeletal network of film that had surrounded the ZnO grains. X-ray diffraction analysis of the residual material showed it to be a mixture of $Zn_7Sb_2O_{12}$ spinel and a Bi-containing pyrochlore of composition $Bi_3Zn_2Sb_3O_{14}$ [4]. Single-phase powder of the $Bi_3Zn_2Sb_3O_{14}$ varistor phase was synthesized by Achard et al. through a novel procedure: direct oxidation of a precursory alloy (DOPA) [6]. A melt of the component metals was propelled through a nozzle with hot compressed air and quenched in a bath of water. The resulting product was a homogenous alloy in the form of pellets of *ca.* 40 μm diameter. The pellets were then oxidized in air under a carefully-controlled sequence of reaction steps that produced single-phase pyrochlore of controlled stoichiometry.

The nonohmic behavior of the varistor is not a consequence of the pyrochlore phase being present at grain boundaries [2]. This has been confirmed by direct

*Present address: Department of Materials Science and Engineering, Pennsylvania State University, University Park, PA 16802, USA.
†Present address: Department of Materials Science, Graduate School of Engineering, Tohoku University, Sendai 980-8579, Japan.

measurements of the I/V characteristics of individual interfaces combined with determination of their chemistry and phase composition [7]. The pyrochlore phase is, nevertheless, of great importance to varistor fabrication. A reversible reaction of the pyrochlore with ZnO

$$2Bi_3Zn_2Sb_3O_{14} + 17ZnO \Leftrightarrow 3Zn_7Sb_2O_{12} + 3Bi_2O_3(l)$$

which progressively proceeds toward completion as the processing temperature is increased, contributes Bi_2O_3 liquid that promotes liquid-phase sintering as well as dissolving other oxides present in the initial varistor formulation. The formation temperature, morphology and composition of the pyrochlore phase has thus been the subject of continued study [8, 9]. It has been suggested that direct use of $Bi_3Zn_2Sb_3O_{12}$ and $Zn_7Sb_2O_{12}$ as starting materials, rather than the individual binary oxides of the components, can reduce the loss of Bi and Sb by vaporization during processing [10].

An ideal pyrochlore has composition $A_2B_2O_7$ where A and B can be a large A^{2+} ion and a smaller B^{6+} species or, more commonly, A^{3+} and B^{4+}. The structure is an ordered superstructure, space group $Fd3m$, that has a lattice constant twice that of a M_4O_8 flourite-like arrangement of atoms. The pyrochlore cell thus contains eight formula units. Six of the oxygen ions per formula unit occupy the $48f$ site of the space group and are tetrahedrally coordinated by 2A and 2B cations. The seventh oxygen ion is located in the 8a site and coordinated by four A cations. This leaves eight anion sites of the parent flourite structure unoccupied. This "vacancy" order in position $8b$ which, if occupied, would be tetrahedrally coordinated by four B cations. The ordered arrangement of unoccupied anion sites leaves A with eight oxygen neighbors (as in the flourite-type structure). The smaller B cation is six-coordinated.

The stoichiometry $Bi_3Zn_2Sb_3O_{14}$ does not permit ordering of the cation species among the sites present in an ideal pyrochlore arrangement. Distorted derivatives and ordered superstructures of the basic pyrochlore structure type are known. X-ray powder diffraction patterns obtained from single phase, high quality $Bi_3Zn_2Sb_3O_4$ powders [6, 12, plus unpublished x-ray and neutron powder diffraction profiles obtained in the present study] indicate a normal pyrochlore structure that, accordingly, must have a disordered arrangement of cations. Mergen and Lee [11, 12] proposed that the site occupancies are $(Bi_{1.5}Zn_{0.5})(Sb_{1.5}Zn_{0.5})O_2$ on the basis of the ionic radii of the cation species. This view was supported by the fact that a single-phase pyrochlore structure was found to be retained when other divalent cations (with preference for centering either the A or B site on the basis of their ionic radii) were substituted for Zn^{2+}. Specifically, $(Bi_{1.5}A_xZn_{0.5-x})(Sb_{1.5}Zn_{0.5})O_7$ solid solutions remained single phase for $0 \leq x \leq 0.5$ when A was Cd^{2+} (but not for Ca^{2+} and Sr^{2+} for $x > 0.1$). Similarly, $(Bi_{1.5}Zn_{0.5})(Sb_{1.5}Mg_xZn_{0.5-x})O_7$ was single phase for $0 \leq x \leq 0.5$ as was a phase with complete double substitution $(Bi_{1.5}Cd_{0.5})(Sb_{1.5}Mg_{0.5})O_7$. Progressive solid solution in a pyrochlore can, in some systems, lead to the mixing of the cations initially present in the A and B site (anti-site cation defects) and also exchange of the oxygen in the $48f$ sites with the empty $8b$ interstices, as has been found in neutron Rietweld analyses of several pyrochlore solid solution systems [13, 14]. The anion exchange creates Frenkel defects whose formation is described in Kröger–Vink notation by the reaction $O_o \leftrightarrow O_i'' + V_o^{\cdot\cdot}$. Such defects will have a major effect on oxygen ion conductivity.

The present work describes an initial study of the electrical conductivity of bulk $Bi_3Zn_2Sb_3O_{14}$ pyrochlore as a function of temperature and oxygen partial pressure using two-probe complex impedance spectroscopy. Oxygen concentration cell measurements were used to determine the ionic transference number, as some pyrochlores are known to exhibit significant levels of ionic conductivity due to either intrinsic Frenkel disorder [15] or acceptor doping [16].

Our primary interest in the electrical properties of $Bi_3Zn_2Sb_3O_7$ pyrochlore arose because of its presence at interfaces in varistor ceramics. It is worth noting, however, that Bi pyrochlores are dielectric ceramics that have been studied for some time [17, 18]. There has been considerable recent interest [19–24] in pyrochlores, with compositions that are very close to that of the material of the present study for applications as Pb-free ceramics with high, thermally stable dielectric constants and small dielectric ions. Values of K can be as large as 250 at 1 MHz [22]. Dielectric loss, $\tan\delta$, is frequently in the range 1×10^{-4}–6×10^{-4}. In addition, the temperature coefficient of the dielectric constant can be either positive or negative and may be tuned to very small values by modification of the composition of the pyrochlore through solid solution; values can range -5×10^{-4} to $+2 \times 10^{-4}$ K^{-1}. For the $Bi_3Zn_2Sb_3O_{14}$ pyrochlore studied in the present work, values of the dielectric constant, K, dielectric loss, $\tan\delta$, and temperature coefficient, τ_K have been reported as $K = 28.4$,

$\tan\delta < 0.001$ and $\tau_K = -58 \times 10^{-6}\ K^{-1}$ at 10 kHz [20] and $K = 32$ and $\tan\delta = 0.005$ at 100 kHz [12]. Substitution of Nb or Ta for Sb results in improved dielectric properties. For $Bi_3Zn_2Nb_3O_{14}$, for example, reported values for K, $\tan\delta$ and τ_K have been 153.1, 0.0140 and $-3.23 \times 10^{-4}\ K^{-1}$, respectively, at 10 kHz [20] and 170, <0.0004 and $-4 \times 10^{-4}\ K^{-1}$ at 1 MHz [23].

Experimental Methods

The $Bi_3Zn_2Sb_3O_{14}$ pyrochlore powder used for this study was synthesized by one of us (R. Metz) by direct oxidation of a precursory alloy (DOPA) using the apparatus and procedure described above [6]. Disks for conductivity measurements were prepared by uniaxially pressing the powder in a 1/4 inch die at 5000 psi (34 mpa). No binder was used. The disks were sintered at 1200°C for 1 hour in a closed alumina crucible at a heating rate of 5°C per minute. The cooling rate was 10°C per minute. The measured density of the pellets ranged from 92% to 95% of theoretical density. The final dimensions of the pellet were, thickness = 3.60 mm and diameter = 5.89 mm. The presence of a single-phase pyrochlore structure for the material was confirmed with X-ray diffraction patterns using a Rigaku 300 diffractometer equipped with a diffracted-beam graphite monochromator (Cu Kα radiation from a rotating anode x-ray tube, $10^\circ \le 2\theta \le 100^\circ$). The pellets were coated with platinum ink (Engelhard #6926) and then fired at 800°C for 2 hours, to provide electrodes for the conductivity measurements.

The electrical conductivity was derived from a complex-plane analysis [25] using Z-probe impedance spectroscopy (Solartron SI 1260 Impedance/gain-phase Analyzer). The frequency was varied between 1 MHz and 0.1 Hz. Measurements were made at several temperatures between 550°C and 1000°C. The partial pressures of oxygen employed ranged from a maximum of 1 atm to a minimum of 10^{-4} atm.

There was concern that Bi_2O_3 or Sb_2O_3 might be lost through vaporization at elevated temperatures (~900°C through 1000°C) and low Po_2. Thermogravimetric analysis (TGA) was thus applied to an unconsolidated powder sample heated to 1000°C in air and then in high purity helium.

A concentration cell was used for the determination of the ionic transference number. A pyrochlore disk was prepared through the procedure described above except that polyethylene glycol was used as a binder. The disk was pressed in a 3/4 inch die at 6000 psi (41 MPa). Additionally, platinum mesh (99% Pt gauze, 52 mesh woven from 0.1-mm diameter wire, Alfa AESAR # 10283) was pressed onto the surface of the pellet at both ends to serve as electrodes. The pellet was heated to 750°C for binder burnout and then sintered at 1200°C for 1 hour. A Pyrex o-ring (softening temperature of 821°C) was used to seal the pellet against a constriction in a quartz tube. A schematic diagram of the cell is shown in Fig. 1. The sample was pushed against the Pyrex

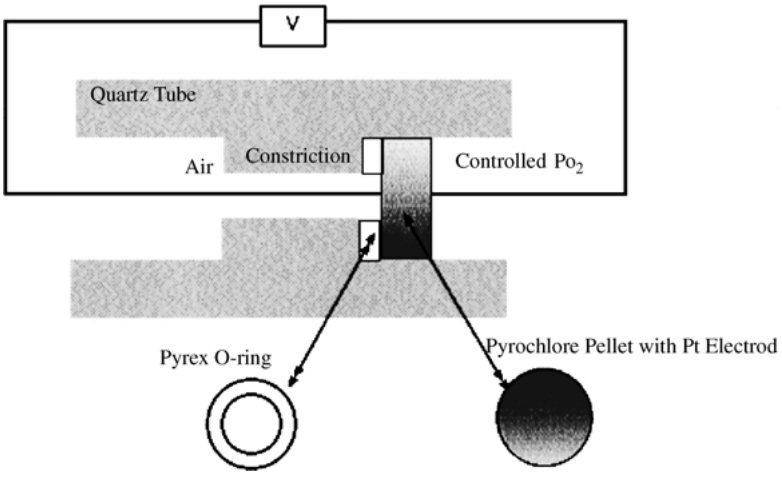

Fig. 1. Schematic diagram of the experimental apparatus that was employed for concentration cell measurements. The emf is measured across the pellet. A Pyrex O-ring seals the pyrochlore disk to a constriction in the quartz tube thereby permitting different oxygen partial pressures to be maintained on either side of the sample.

o-ring and the assembly was then heated to the softening temperature, thus sealing the pellet to the constriction in the quartz tube. For the cell measurement, one side of the pellet was exposed to air and the other side to a series of different oxygen partial pressures. The emf of the cell was measured at 800°C as a function of Po_2.

Results

The electrical conductivity was measured at temperatures ranging from 550°C to 1000°C. Achievement of equilibrium with the atmosphere was difficult at temperatures <700°C due to slow kinetics. Our TGA results indicated a likely loss of Bi_2O_3 at temperatures greater than ~900°C. A lack of reversibility in the conductivity measurements performed at elevated temperatures supported this conclusion. Due to these limitations at both low and high temperatures, equilibrium conductivity measurements were limited to temperatures between 750 and 850°C. Furthermore, due to the apparent Bi_2O_3 loss at Po_2 less than 10^{-4} atm, conductivity measurements were further confined to a Po_2 range of 1 atm to 10^{-4} atm.

Figure 2 shows a typical complex impedance plot that was obtained for the $Bi_3Zn_2Sb_3O_{14}$ pyrochlore. This spectrum is dominated by a semicircle with a high frequency intercept at the origin suggesting that the source of the dispersion is a parallel arrangement of the bulk resistance and capacitance. This assignment was confirmed by noting that the relative dielectric constant extracted from the capacitance was equal to ~25–32 in the temperature range between 550 and 650°C, a value typical for the bulk dielectric constant in pyrochlores [15]. An additional small contribution that we attribute to the electrode impedance is evident at the lowest frequencies. No attempt was made to confirm this as this contribution plays no role in our interpretation. In addition, no distinct grain boundary contribution is evident. Figure 2 is typical of all of the complex impedance plots that were obtained.

Figure 3 presents isotherms of log σ as a function of log Po_2 obtained at temperatures of 750, 800, and 850°C. The range of oxygen partial pressure extends from 1 to 10^{-4} atm. Under the most oxidizing atmospheres, the pyrochlore exhibits a conductivity that increases with increasing Po_2. This is characteristic of *p*-type conduction. At intermediate Po_2, a very shallow minimum occurs. This minimum is followed by increasing conductivity upon further decrease in Po_2, consistent with *n*-type conduction. The presence of the shallow minimum indicates mixed ionic-electronic conduction. Also apparent is a distinct shift of the conductivity minimum to higher Po_2 with increasing temperature. This shift indicates a significant difference in the activation energies for *n*-type and *p*-type conduction.

Assuming a model in which intrinsic ionic disorder in the form of anion Frenkel defects predominates [15], then

$$O_O \leftrightarrow V_O^{\cdot\cdot} + O_i'' \qquad [O_i''][V_O^{\cdot\cdot}] = K_F(T) \qquad (1)$$

At high Po_2, the oxidation reaction for the removal of oxygen vacancies and the creation of holes is

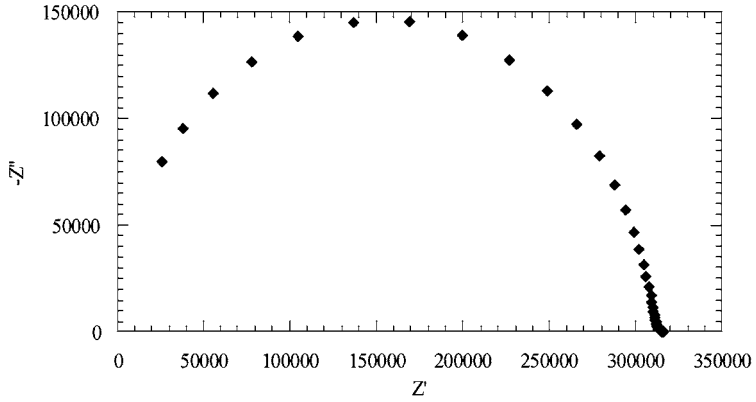

Fig. 2. Complex impedance plot of data recorded as a function of frequency at 600°C in air. The intersection of the large semicircle with the real axis is taken as the bulk resistance. There is no evidence of a distinct contribution by grain boundaries. An electrode contribution at the maximum value of Z' is barely detectable.

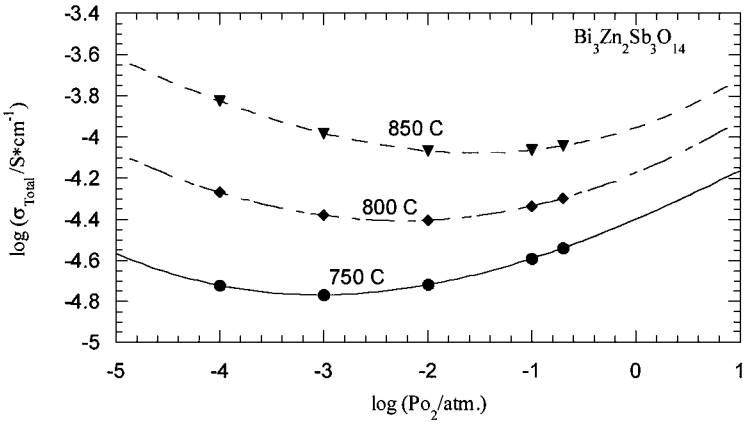

Fig. 3. Isotherms of the total electrical conductivity of $Bi_3Zn_2Sb_3O_{14}$ as a function of the logarithm of oxygen partial pressure. The curves passed through the data are fits of the relation predicted by Eq. (5).

given by

$$V_O^{\cdot\cdot} + 1/2O_2(g) \leftrightarrow O_O + 2h^{\cdot}. \quad p^2/[V_O^{\cdot\cdot}]\,Po_2^{1/2} = K_{ox} \tag{2}$$

Similarly, at low Po_2, the reduction reaction for the creation of oxygen vacancies and electrons is given by

$$O_O \leftrightarrow V_O^{\cdot\cdot} + 1/2O_2(g) + 2e'. \quad n^2[V_O^{\cdot\cdot}]\,Po_2^{1/2} = K_R \tag{3}$$

where K_F, K_{ox} and K_R are the appropriate equilibrium constants. Applying the above mass-action relations and the requirement for electroneutrality (n, p assumed $\ll [V_O^{\cdot\cdot}]$, $[O_i'']$, given high ionic intrinsic disorder commonly observed in pyrochlores [13, 15])

$$[V_O^{\cdot\cdot}] = [O_i''] = (K_F)^{1/2} \tag{4}$$

the n-type conduction can be readily shown [26] to have a $Po_2^{-1/4}$ dependence, p-type conduction a $Po_2^{1/4}$ dependence, and the ionic conductivity, without Po_2 dependence. The total conductivity, σ, thus will be given by:

$$\sigma_T = \sigma_n^o\,(Po_2)^{-1/4}\,\exp\left(\frac{-E_n}{kT}\right) + \sigma_p^o\,(Po_2)^{1/4} \times \exp\left(\frac{-E_p}{kT}\right) + \frac{\sigma_i^o}{T}\,\exp\left(\frac{-E_i}{kT}\right). \tag{5}$$

The curves that have been passed through the conductivity measurements in Fig. 3 represent the best fit of Eq. (5) to the date. The relation provides an excellent description of the experimental results. The values of the pre-exponential terms and the activation energies that were employed in obtaining the fit are summarized in Table 1.

Oxygen concentration cell measurements were performed at 800°C. The cell voltage, E, is plotted in Fig. 4 as a function of the logarithm of oxygen partial pressure. The average ionic transference number, $\bar{t}_i$, can be determined from the relation

$$E = \bar{t}_i\,\frac{kT}{4e}\,\ln\left[\frac{Po_2''}{Po_2'}\right] \tag{6}$$

where Po_2'' and Po_2' correspond to the partial pressures of oxygen on either side of the sample. However, a more precise method for determination of the ionic transference number at each Po_2 is to employ a differential

Table 1. Pre-exponential and activation energy terms corresponding to Eq. (5).

	σ_o, Pre-exponential term (S/cm)	ΔE, Activation energy (eV)
n-type contribution	7.59×10^5	2.41 ± 0.4
p-type contribution	1.45×10^{-1}	0.74 ± 0.5
Ionic contribution	9.44×10^5	1.67 ± 1.0

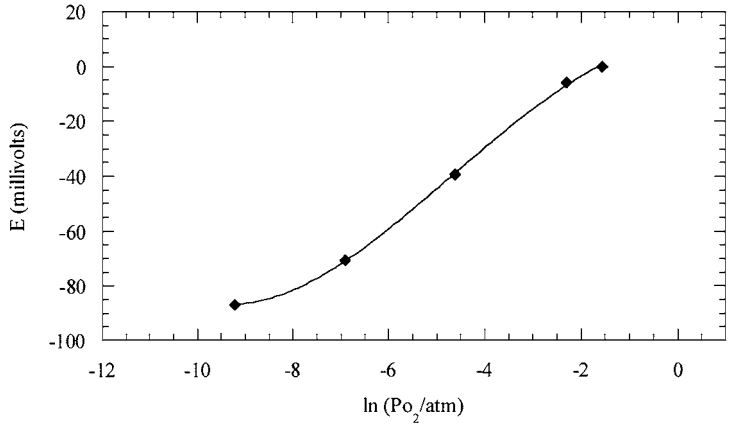

Fig. 4. Concentration cell emf measured at 800°C as a function of the variable oxygen partial pressure, Po_2'', applied to one surface of the specimen. The reference partial pressure, Po_2, was air. The ionic transference number, t_i; was determined from the slope of the curve using Eq. (7).

form of Eq. (6) [26]:

$$\left.\frac{dE}{d(\ln Po_2)}\right|_{(Po_2=Po_2'')} = t_i(Po_2'')\frac{kT}{4e} \qquad (7)$$

where Po_2', the reference partial pressure, is held constant (air for the present measurements). Figure 5 presents the variation of the ionic transference number, t_i, as obtained by Eq. (7), as a function of oxygen partial pressure, Po_2''. The maximum value of t_i is approximately 0.35.

The ionic transference number may also be evaluated by use of the expressions for ionic conductivity and for *p*- and *n*-type electronic conductivity that were obtained by fitting the conductivity isotherms by Eq. (5) (Fig. 3). The values of t_i that result from such analysis, when applied to the conductivity data obtained at

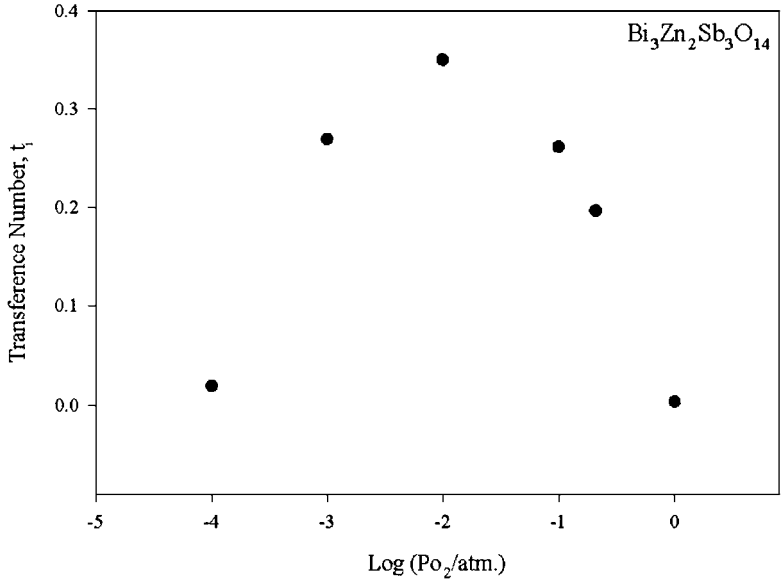

Fig. 5. Values of the ionic transference number, t_i, at 800°C, plotted as a function of oxygen partial pressure. The values of t_i were determined from the slope of the emf versus Po_2'' curve.

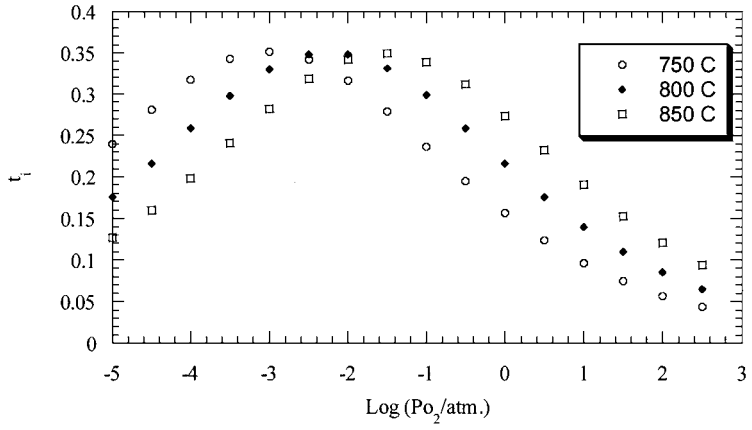

Fig. 6. Variation with log Po_2 of ionic transference numbers evaluated from the temperature and oxygen partial-pressure dependence of t_n, t_p and t_i. These expressions had been derived from fits to conductivity isotherms measure as a function of Po_2.

750, 800 and 850°C, are plotted as a function of the logarithm of Po_2 in Fig. 6. There is a good agreement between the results obtained in this fashion from the 800°C conductivity data and the values of t_i directly determined from the concentration cell measurements. It may be noted from Fig. 6 that the maximum in the values for t_i progressively shifts to higher oxygen partial pressures as temperature is increased. This occurs for exactly the same reason that the minimum in the total conductivity, Fig. 3, shifts to higher Po_2: namely, the more rapid increase with temperature of n-type conductivity relative to p-type as a consequence of the smaller activation energy of the latter.

Discussion

The electrical conductivity of $Bi_3Zn_2Sb_3O_{14}$ pyrochlore, measured under equilibrium conditions for several isotherms, was found to exhibit a transition from n-type to p-type conductivity with increasing Po_2 characterized by a rather shallow conductivity minimum. Furthermore, an ionic transference number of 0.35 at $Po_2 \sim 10^{-2}$ atm. at 800°C confirms a significant ionic contribution. This maximum in the ionic transference number is consistent with the minimum shown in the conductivity data for 800°C. Both the concentration cell measurements and the conductivity data are consistent with a defect model based on oxygen frenkel disorder and further confirm a non-negligible ionic contribution to the conductivity.

The values of the activation energies for n-type and p-type conduction determined from the fit were 2.41 ± 0.4 eV and 0.74 ± 0.5 eV respectively. These values demonstrate the significant difference between the energies for p-type and n-type conduction, as did the shifting conductivity minimum with increasing temperatures. Based on the above defect model, the n-type activation energy is one half the enthalpy of reduction ($H_R = 4.82 \pm 0.8$ eV) while the p-type activation energy is one half the enthalpy of oxidation ($H_{ox} = 1.48 \pm 1.0$ eV). This assumes non-activated electron and hole carrier mobilities, a not unreasonable assumption for Zn-based oxides.

The ionic activation energy, E_i, represents the sum of defect formation ($H_F/2$) and migration (H_{mig}) enthalpies ($H_F/2 + H_{mig} = 1.67 \pm 1.0$ eV). There is good evidence that cation disordered pyrochlores ($A \leftrightarrow B$ exchange) also exhibit a high level of intrinsic oxygen frenkel disorder ($48f \rightarrow 8b$) [13–15]. This would suggest that H_F is small and that the majority of the activation energy for ionic conductivity is tied to the migration term. This suggestion requires further study. The relatively large error bars on E_i are a consequence of the small number of isotherms (3) that could be examined in a reproducible manner. Nevertheless, the good agreement between the conductivity and ionic transference measurements provides additional confidence to the relative accuracy of the data.

The np product is known to be a constant given by

$$np = N_C N_V \exp\left[-\frac{E_g}{kT}\right] \tag{8}$$

where N_C and N_V are the conduction and valence bond density of states and E_g the band energy. It therefore

follows that the sum $E_n + E_p$, assuming non-activated carrier mobilities, equals the band gap energy E_g. For $Bi_3Zn_2Sb_3O_{14}$, we thus estimate E_g to be equal to 3.15 ± 0.9 eV.

Conclusion

The first equilibrium transport studies of $Bi_3Zn_2Sb_3O_{14}$ pyrochlore have shown the material to be a mixed ionic-electronic conductor. This is supported by the Po_2 dependence of the conductivity and the ionic transference number measurements. *P*-type conductivity dominates at high Po_2, under oxidizing conditions, and *n*-type conductivity dominates at low Po_2, under reducing conditions. Additionally, a considerable ionic contribution to the conductivity is apparent due to the presence of the shallow minimum in conductivity measurements. The presence of this contribution was confirmed with the results of the concentration cell measurements. Employing a model in which Frenkel defects are assumed to be dominant, permitted the extraction of a number of key thermodynamic and kinetic data from the electrical conductivity data. Such results include the enthalpies of reduction, oxidation, the sum of oxygen vacancy formation and migration and the band gap energy.

Acknowledgments

This work was supported by the Department of Energy, Basic Energy Sciences under contract #DE-FG02-86ER45261. The results contributed to the present paper by one of us (Jane Clayton) were obtained during a Summer Internship supported by a National Science Foundation Research Experiences for Undergraduates (REU) program. This grant is provided as a supplement to a Materials Research Science and Engineering Center (MRSEC) award to MIT's Center for Materials Science and Engineering, DMR 9808941. Gratitude is also expressed to the MIT Materials Processing Center for funding to meet her travel expenses. We are indebted to Alain Marchand, Henri Delalu and Jean Jacques Counioux for assistance in the synthesis of the pyrochlore powder.

References

1. M. Matsuoka, *Japanese J. Appl. Phys.*, **10**, 736 (1971).
2. M. Inoda, *Japanese J. Appl. Phys.*, **19**, 409 (1980).
3. E. Olsson, L.K.L. Falk, G.L. Dunlop, and R. Osterbund, *J. Mater. Sci.*, **20**, 4091 (1985).
4. J. Wong, *J. Appl. Phys.*, **46**, 1653 (1975).
5. J. Wong, *J. Am. Ceram. Soc.*, **57**, 357 (1974).
6. N. Achard, J.-J. Counioux, and A. Marchand, *Eur. J. Solid State Inorg. Chem.*, **34**, 425 (1997).
7. E. Olsson and G.L. Dunlop, *J. Appl. Phys.*, **66**, 3666 (1989).
8. J.C. Kim and E. Goo, *J. Mater. Sci.*, **24**, 76 (1989).
9. L. Karanovi, D. Poleti, and D. Vaović, *Mater. Lett.*, **18**, 191 (1994).
10. R. Metz, H. Delalu, J.R. Vignalou, N. Achard, and M. Elkhatib, *Mater. Chem. Phys.*, **63**, 157 (2000).
11. A. Mergen and W.E. Lee, *J. Eur. Ceram. Soc.*, **16**, 1041 (1996).
12. A. Mergen and W.E. Lee, *Mater. Res. Bull.*, **32**, 175 (1997).
13. C. Heremans, B.J. Wuensch, J.K. Stalick, and E. Prince, *J. Solid State Chem.*, **117**, 108 (1995).
14. B.J. Wuensch, K.W. Eberman, C. Heremans, E.M. Ku, P. Onnerud, E.M.E. Yeo, S.M. Haile, J.K. Starlick, and J.D. Jorgensen, *Solid State Ionics*, **129**, 111 (2000).
15. P.K. Moon and H.L. Tuller, *Solid State Ionics*, **28–30**, 470 (1988).
16. S. Kramer and H.L. Tuller, *Solid State Ionics*, **82**, 15 (1995).
17. G.I. Golovshchikova, V.A. Isupov, A.G. Tutor, I.E. Mylnikova, P.A. Nikitina, and O.I. Tulinova, *Sov. Phys. - Solid State*, **14**, 2539 (1973).
18. G. Jeanne, G. Desgardin, and B. Raveau, *Mater. Res. Bull.*, **9**, 1321 (1974).
19. H.C. Ling, M.F. Yan, and W.W. Rhodes, *J. Mater. Res.*, **5**, 1752 (1990).
20. J.C. Champarnaud-Mesjard, M. Manier, B. Frit, and A. Tairi, *J. Alloys Compd.*, **88**, 174 (1992).
21. D. Liu, Y. Liu, S.-Q. Huang, and X. Yao, *J. Am. Ceram. Soc.*, **76**, 2129 (1993).
22. D.P. Cann, C.A. Randall, and T.R. Shrout, *Solid State Comm.*, **100**, 529 (1996).
23. X. Wang, H. Wang, and X. Yao, *J. Am. Ceram. Soc.* **80**, 2745 (1997).
24. M. Valant and P.K. Davies, *J. Am. Ceram. Soc.*, **83**, 147 (2000).
25. I.M. Hodge, M.D. Ingram, and A.R. West, *J. Electroanal. Chem.*, **74**, 125 (1976).
26. H.L. Tuller, in *Nonstochiometric Oxides*, edited by O.T. Sorenson (Academic Press, New York, 1981), p. 271.